Monthly Notices
of the
ROYAL ASTRONOMICAL SOCIETY

MNRAS **444,** 620–628 (2014) doi:10.1093/mnras/stu1481

On the Class II methanol maser periodic variability due to the rotating spiral shocks in the gaps of discs around young binary stars

S. Yu. Parfenov★ and A. M. Sobolev

Ural Federal University, 51 Lenin Str., Ekaterinburg 620000, Russia

Accepted 2014 July 22. Received 2014 July 17; in original form 2014 June 20

ABSTRACT

We argue that the periodic variability of Class II methanol masers can be explained by variations of the dust temperature in the accretion disc around protobinary star with at least one massive component. The dust temperature variations are caused by rotation of hot and dense material of the spiral shock wave in the disc central gap. The aim of this work is to show how different can be the Class II methanol maser brightness in the disc during the Moment of Maximum Illumination by the Spiral Shock material (MMISS) and the Moment when the disc is Illuminated by the Stars Only (MISO). We used the code CLOUDY (v13.02) to estimate physical conditions in the flat disc in the MISO and the MMISS. Model physical parameters of the disc were then used to estimate the brightness of 6.7, 9.9, 12.1 and 107 GHz masers at different impact parameters p using large velocity gradient approximation. It was shown that the strong masers experience considerable brightness increase during the MMISS with respect to MISO. There can happen both flares and dips of the 107 GHz maser brightness under the MMISS conditions, depending on the properties of the system. The brightest 9.9 GHz masers in the MMISS are situated at the greater p than the strong 6.7, 12.1 and 107 GHz masers that are situated at $p < 200$ au. The brightness of 9.9 GHz maser in the MMISS suppressed at $p < 200$ au and increase at $p > 200$ au.

Key words: accretion, accretion discs – masers – binaries: general.

1 INTRODUCTION

Class II methanol masers are widespread in the regions of star formation (Caswell 2013). There are several hypotheses on the sites of the Class II methanol masers formation. First maser sources of this type were found towards ultracompact H II regions (Wilson et al. 1984) and for some sources this association has been confirmed interferometrically (see e.g. Menten et al. 1992; Walsh et al. 1998). Indeed, Class II methanol masers can be excited by emission of the youngest H II regions with high emission measure (Slysh, Kalenskiĭ & Val'tts 2002; Sobolev et al. 2007). Another hypothesis about association of Class II methanol masers with accretion discs was suggested by Norris et al. (1998) and finds support in interferometric observations (e.g. Moscadelli & Goddi 2014; Sugiyama et al. 2014). Actually, these two hypotheses are not in contradiction because photoevaporation of discs around massive stars can give birth to the youngest H II regions (Hollenbach et al. 1994). In the case of discs the maser pumping is greatly influenced by the dust emission which has high potential to produce bright masers (Sobolev, Cragg & Godfrey 1997; Voronkov et al. 2005). According to the other hypothesis Class II methanol masers are formed in the outflows from the young stellar objects (e.g. De Buizer et al. 2009). The masers in the outflows can be pumped by the heated dust. In fact it is often very difficult to discriminate between the disc and the outflow sites from the maser observations (Minier, Booth & Conway 2000; van der Walt, Sobolev & Butner 2007) and even by combination of the maser and non-maser observations (e.g. Edris et al. 2005) because the outflow forms at the disc surface.

Some of Class II methanol maser sources associated with massive star formation regions show periodic variability. There could be different mechanisms underlying variability of such kind (see e.g. Goedhart, Gaylard & van der Walt 2005a). It is more likely that these mechanisms have radiative nature (Goedhart et al. 2005b).

One of such mechanisms is proposed by van der Walt (2011) and it relates the maser variability with background variations. Background variations itself are caused by the variability of colliding winds in a massive binary.

Other possible mechanism is related with variations of the dust infrared emission that is believed pumps Class II methanol masers (Sobolev & Deguchi 1994). As it was shown by Cragg, Sobolev & Godfrey (2005) the brightness temperature of Class II methanol masers could be very sensitive to variations of temperature of the dust T_d that is the source of pumping infrared emission.

Inayoshi et al. (2013) suggested that dust temperature variations could be caused by pulsations of a massive protostar growing under

★ E-mail: sergey.parfenov@urfu.ru

high accretion rates. Araya et al. (2010) explained T_d variations by the variability of the accretion rate of the disc material on to a young binary system. Goedhart et al. (2014) also claim that maser flare properties could be explained by binarity of a star associated with variable maser sources.

At the moment there are no strong evidences that the Class II methanol masers in any variable source with confirmed periodicity reside in the circumstellar disc. However, number of indications on that increases. For example, periodic variability was recently found in Cepheus A by Szymczak, Wolak & Bartkiewicz (2014). The Class II methanol masers in this source most probably reside in the ring that is perpendicular to the jet associated with the radio continuum source Hughes and Wouterloot 2 (HW2; Torstensson et al. 2011).

In this paper we consider possibility to explain periodic methanol maser phenomena in the model with the masers produced in accretion disc containing binary system and rotating spiral shocks in its central cavity. The structure of the circumbinary disc around low-mass young binaries was studied by Ochi, Sugimoto & Hanawa (2005), Sytov et al. (2011) and Gómez de Castro et al. (2013). We assume that the similar disc structure is possible in the case of a binary with massive components (see e.g. Krumholz et al. 2009).

The considered accretion disc structure has the relatively small gap in the centre that is filled by the low-density very hot gas and rotating spiral shocks (bow shocks) formed due to supersonic motion of binary components. The rotation of the bow shock leads to periodical changes in the radiation field within parts of the disc illuminated by the shock. This in turn leads to dust temperature variations in these parts of the disc. We used the simple disc model to estimate how the brightness of Class II methanol masers in the accretion disc could be affected by the bow shock illumination.

2 DISC MODEL

2.1 General description

We consider the case when Class II methanol masers are formed in the accretion disc around the protobinary star containing massive and intermediate-mass stars. There is a gap in the disc centre formed by rotating bow shocks. We assume that the gas in the accretion disc is in thermal and ionization equilibrium.

Luminosity and spectrum of the radiation in some radial direction are subject to variations due to the rotation of the bow shock. The material behind the bow shock is hot, dense and luminous in the ultraviolet and optical range, depending on the shock speed. The maximums of density and temperature of the material behind the bow shock are located in the bow shock base, i.e. the shocked region close to the surface of the massive protobinary component. The value of gas column density, N_{gas}, computed along the line of sight between the disc centre and the outer disc boundary (excluding the stellar material) attains its maximum when the bow shock base is on this line of sight (Sytov et al. 2009). The luminosity of the radiation that strikes the inner accretion disc boundary is maximum when the boundary is illuminated by the material close to the bow shock base and this corresponds to the Moment of Maximum Illumination by the Spiral Shock material (MMISS).

The rotation of the spiral shock wave material causes relevant change of T_d in the disc. This change of T_d affects the pumping of methanol maser and thus leads to the maser variability.

To estimate the maser brightness in the accretion disc in the Moment when the disc is Illuminated by the Stars Only (MISO) and in the MMISS we used two models. The first model includes the disc and the protobinary stellar system that is in the disc central gap (Fig. 1a). In the second model we introduce a shocked gas layer that partially fills the space between the accretion disc inner boundary and the massive component (Fig. 1b). This gas layer modifies the massive star radiation before it strikes the inner disc boundary and produces great amount of radiation itself. The radiation of the intermediate-mass component is not included in the second model because it is eclipsed by the massive component.

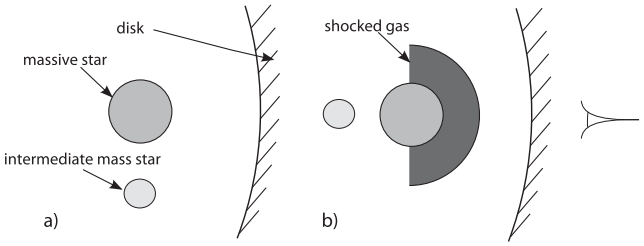

Figure 1. The schematic view of two models: (a) in the MISO; (b) in the MMISS. The difference of protobinary components positions relatively to the disc inner boundary is only for clarity and was not accounted for in the calculations.

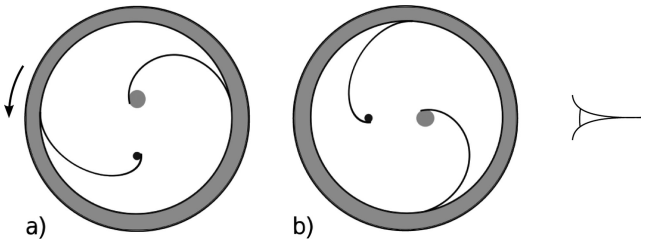

Figure 2. The schematic view of protobinary and spiral shocks configurations in the disc inner gap for two time moments which differ by the half of the binary orbital period. Filled circles show positions of protobinary components, arcs correspond to the bow shocks and the ring corresponds to the inner boundary of circumbinary disc. The arrow indicates the direction of binary, disc and bow shocks rotation. (a) In the MISO. (b) In the MMISS.

These two models mimic binary and spiral shocks configurations similar to those presented in Fig. 2. The eclipse of the massive protobinary component by the intermediate-mass component is not considered in this study. Also we do not account for the bow shock borne by the intermediate-mass component and for variations of dilution factors due to orbital motion of protobinary components.

2.2 Modelling with CLOUDY

To estimate physical conditions in the circumbinary accretion disc and to compute the radiation intensity from the spiral shock material we used the photoionization code CLOUDY version C13.02 (Ferland et al. 2013). To compute physical parameters of the accretion disc under the MISO conditions we used following CLOUDY input parameters.

(i) Central stars. The massive star and intermediate-mass star. Massive star has the mass $M = 13\,M_\odot$, effective temperature $T_{eff} = 29\,000$ K, surface gravity $\log g = 4.2$ dex, bolometric luminosity $L = 14295\,L_\odot$ and solar metallicity (Grevesse & Sauval 1998). The atmosphere model for this star was taken from the Lanz & Hubeny (2003) grid of stellar atmosphere models. Intermediate-mass star has $M = 7\,M_\odot$, $T_{eff} = 20\,000$ K, $\log g = 4.2$ dex, $L = 1741\,L_\odot$, solar metallicity and atmosphere model from the Castelli & Kurucz (2004) grid. Stellar luminosities and radii were

obtained for the given log g, $T_{\rm eff}$ and M values. Combined radiation of both stars is represented by the sum of their radiation fields from the central stellar source.

(ii) Geometry of the disc is flat.

(iii) Inner disc radius is assumed to be 1.9 au. This radius is roughly equal to the size of the central disc gap estimated for a binary with components mass ratio of 0.54 and semimajor axis of the binary equal to 1.145 au. The estimate was obtained by linear extrapolation of values calculated by Artymowicz & Lubow (1994) in the framework of resonance theory.

(iv) Outer disc radius is 1000 au which is close to the value obtained by Preibisch et al. (2011) from their observations of the circumstellar disc around massive young stellar object in the Carina nebula.

(v) Disc semiheight is 0.38 au. This value was obtained with the ratio of the height of the disc to its inner radius equal to 0.2, which corresponds to the estimate obtained by Preibisch et al. (2011).

(vi) Chemical composition of the disc is the subjective mean of the Orion nebula abundances determined by Baldwin et al. (1991), Rubin et al. (1991), Osterbrock, Tran & Veilleux (1992) and Rubin, Dufour & Walter (1993). We use the CLOUDY abundance set for H II regions.

(vii) We assume that the dust has CLOUDY built-in grain properties that were obtained for the Orion nebula by Baldwin et al. (1991). Grain physics described by Baldwin et al. (1991) and van Hoof et al. (2004). Graphite and silicate grains distributed in 10 size bins are included in our calculations. The minimum radius of graphite and silicate grains is 0.03 μm while the maximum radius is 0.25 μm. The dust-to-gas mass ratio is 0.005. In order to simulate sublimation of the dust grains we weight dust abundance with the temperature $\exp\left[-(T_{\rm d}/T_{\rm sub})^2\right]$, where $T_{\rm sub}$ is the sublimation temperature for a given grain size and chemical composition. The dependence of gas-to-dust ratio on the dust temperature was chosen to provide good convergence of CLOUDY calculations.

(viii) Additional heating due to the viscous dissipation H is treated in the framework of α-disc model (Shakura & Sunyaev 1973):

$$H = \alpha P \sqrt{\frac{GM}{r^3}}, \tag{1}$$

where α – dimensionless parameter of the α-disc model which is held constant over the disc; P – local gas pressure; G – gravitational constant; M – total mass of the binary; r – distance to the disc centre. We made calculations with $\alpha = 0.00008$ and 0.05 which were, respectively, minimum and maximum values of α obtained by McClure et al. (2013) by fitting spectral energy distributions of classical T Tauri stars.

(ix) Hydrogen number density (the sum of number densities of ionized, neutral, molecular and other hydrogen varieties) $n_{\rm H}$ is proportional to inverse disc radius r^{-1}. This is consistent with the estimates of Ilee et al. (2013) for the surface density distribution in the discs around massive stars under assumption that the surface density profile is close to the number density profile. The hydrogen number density at the inner disc edge is $10^{9.8}$ cm^{-3}. Such density distribution along with the chosen stellar parameters allows to obtain high model brightness of 6.7 and 12.1 GHz Class II methanol masers (see Section 3 for details on maser brightness calculations).

Our assumption on the ionization equilibrium of the gas at the disc inner boundary is valid for the disc with the chosen parameters. This is realized due to the high hydrogen density at the inner disc edge which corresponds to the hydrogen recombination time of about tens of minutes which is small compared to the binary orbital period.

Stellar masses and semimajor axis of the binary were chosen to obtain supersonic velocity for the orbital motion of the massive component and the binary orbital period equal to 100 d. Such period is close to observed values.

CLOUDY input parameters to mimic physical state of the disc under the MMISS conditions are almost the same. The difference is that the disc is illuminated by combined emission of the shocked dust-free gas layer that is located in a central disc gap and the massive stellar component. This seed radiation is computed with CLOUDY assuming that the shocked gas layer has the constant density and temperature. The geometry of this layer is half of a flat disc with the inner radius and semiheight of 0.022 au (radius of the massive star), outer radius of 0.2 au. We made calculations for two shocked gas layer densities $n_{\rm H} = 10^{13.62}$ and $10^{13.32}$ cm^{-3}. Along with the outer layer radius this increases $N_{\rm gas}$ by a factor of ∼100 and ∼50, respectively, compared to $N_{\rm gas}$ in the model without this layer. These column density jumps are consistent with those obtained by Sytov et al. (2009). The shocked gas layer temperature is 30 222 K. This temperature equals the post-shock temperature $T_{\rm s}$ calculated as (Lang 1980)

$$T_{\rm s} = \frac{3}{16}\frac{\mu m_{\rm H} v_{\rm s}^2}{k_{\rm B}}, \tag{2}$$

where $m_{\rm H}$ – hydrogen atom mass; μ – mean molecular weight (for considered chemical composition it is ∼0.7 assuming that the gas is ionized); $k_{\rm B}$ – Boltzmann constant; $v_{\rm s}$ – shock velocity equal to 43.6 km s^{-1} corresponds to the linear velocity of the massive component motion on the circular orbit. It should be noted that in reality the gas temperature behind the bow shock is not constant. The dense gas behind the shock effectively and quickly cools by intense radiation. The cooling efficiency decreases as the gas density rapidly decreases behind the bow shock. The cooling rate also decreases with decreasing gas temperature. Thus, the gas layer with temperature close to $T_{\rm s}$ could be very narrow and located just immediately behind the moving bow shock. But the density and temperature of this layer are close to maximum and it should considerably affect the radiation that illuminates the inner disc boundary.

The approach of the hot shocked gas layer increases bolometric luminosity of the radiation which illuminates the inner boundary of the disc. The increase of the bolometric luminosity reaches ∼18 and ∼27 times if the shocked gas densities are $n_{\rm H} = 10^{13.32}$ and $10^{13.62}$ cm^{-3}, respectively.

One can find more details of computational procedure and CLOUDY input scripts in Appendix A.

2.3 Physical conditions in the disc

It follows from calculations of Cragg et al. (2005) that the high brightness of Class II methanol masers could be attained only when the gas density is lower than 10^9 cm^{-3} and the pumping dust temperature exceeds 100 K. This dust temperature is close to a limit for methanol thermal desorption (Nakagawa 1980; Green et al. 2009). The disc region with such dust temperature and gas density is located at the range of distances from 12 to 120 au from the disc centre under the MISO conditions and from 12 to 400 au under the MMISS conditions. Hereafter, we will call the latter disc region as the disc region with potential for maser formation. Hydrogen number density and gas kinetic temperature in this region calculated for

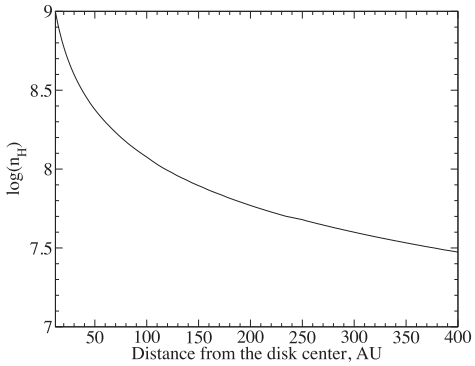

Figure 3. Hydrogen number density (in cm^{-3}) distribution in the disc region with potential for the maser formation.

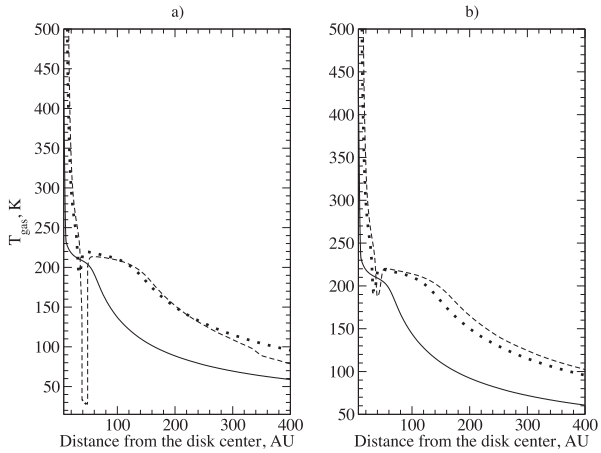

Figure 4. The gas kinetic temperature in the disc region with potential for maser formation in the MISO (solid line) and when there is shocked gas layer in the disc centre with $n_H = 10^{13.32}$ cm^{-3} (dotted line) and $n_H = 10^{13.62}$ cm^{-3} (dashed line). (a) Disc models computed with $\alpha = 0.00008$. (b) Disc models computed with $\alpha = 0.05$.

models with and without shocked gas layer in the disc centre are shown in Figs 3 and 4, respectively.

In Fig. 4 it could be seen that α value has significant influence on the gas kinetic temperature distribution in the disc. In the case of small α and when shocked gas layer with $n_H = 10^{13.62}$ cm^{-3} presents in the disc centre there is the thin disc region with relatively low gas kinetic temperature. It is caused by the thermal front where the gas changes its ionization state and transits to a different branch of the cooling curve (see CLOUDY documentation). When the shocked gas density is equal to $n_H = 10^{13.32}$ cm^{-3} the thermal front is not so apparent. The temperature in this case is mostly the same as in the case of higher shocked gas density.

The dust temperature depends on its chemical composition and size. The temperature for smallest (grain radius of 0.03 μm) considered silicate grains in the disc region with potential for maser formation is presented in Fig. 5. As it was shown by Ostrovskii & Sobolev (2002) a pumping dust composed of such small silicate grains is able to reproduce Class II methanol masers observed patterns. The temperature of graphite grains is presented in Fig. 6. The temperature of the silicate and graphite grains of other sizes is somewhat greater than the shown values.

As it could be seen from Figs 5 and 6 the illumination of the disc by the hot bow shock material leads to the increase of the dust temperature. In our model the dust in the disc region with potential

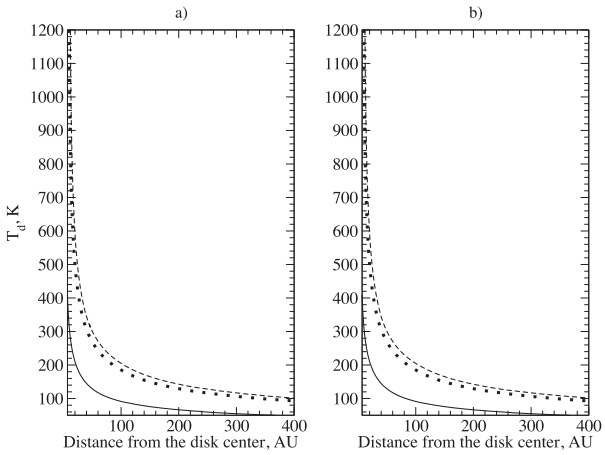

Figure 5. The temperature of small (grain radius of 0.03 μm) silicate grains in the disc region with potential for the maser formation under the MISO conditions (solid line) and when there is shocked gas layer in the disc centre with $n_H = 10^{13.32}$ cm^{-3} (dotted line) and $n_H = 10^{13.62}$ cm^{-3} (dashed line). (a) Disc models computed with $\alpha = 0.00008$. (b) Disc models computed with $\alpha = 0.05$.

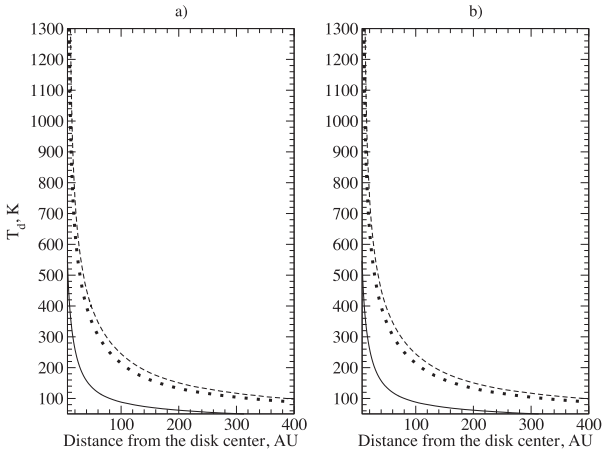

Figure 6. Same as in Fig. 5 but for small graphite grains.

for maser formation is heated mostly by diffuse emission. The dust heating rate due to diffuse emission is of order of 10^{-13} erg s^{-1} cm^{-3}. In this case the time of the dust temperature increase by 10 K is of the order of a few hours. The time of the gas temperature increase should be small compared to the binary orbital period as the thermal equilibrium between the dust and gas establishes quickly at high gas densities. Thus, our assumption on thermal equilibrium of the disc material is valid.

The dust temperature jump in the MMISS allows to preserve high methanol abundance even if the dust temperature falls below 100 K under the MISO conditions. This is because the characteristic time of methanol abundance changes greatly exceeds the binary orbital period.

The dust temperature is almost independent on the α value. This means that in the case of low disc viscosity there could be a disc region where both low gas kinetic temperature and high dust temperature could be realized simultaneously. Such conditions are preferable for creation of extremely bright masers because the greater the difference between gas and dust temperatures, the higher the brightness of 6.7 GHz maser (Cragg et al. 2005). Thus, in our

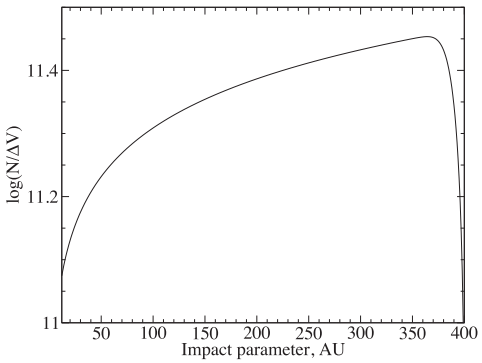

Figure 7. The specific column density (in cm^{-3} s) distribution.

model α is the important parameter which can greatly affect the maser brightness in the accretion disc.

3 MODELLING CLASS II METHANOL MASER EMISSION

For estimated physical conditions in the accretion disc we obtained optical depths and excitation temperatures of Class II methanol masers at different impact parameters to estimate the probability of the maser action at 6.7, 9.9, 12.1 and 107 GHz. The main assumptions for these calculations were the following:

(i) the disc is observed edge on;
(ii) physical conditions are constant along the line of sight and are the same as at the distance from the disc centre that is equal to a given impact parameter.

We used the approach from Sobolev & Deguchi (1994) to compute maser optical depths and excitation temperatures. Line transfer was treated in the large velocity gradient approximation. Input parameters of this model were the spectrum of pumping radiation, gas kinetic temperature, hydrogen number density, beaming factor and specific column density $N_{\rm M}/\Delta V$. The specific column density displayed in Fig. 7 was obtained assuming Gaussian shape of maser lines as

$$\frac{N_{\rm M}}{\Delta V} = \frac{X_{\rm M} f}{\Delta V \epsilon^{-1}} \int_0^{L(p)} n_{\rm H}(l) \exp\left(-\frac{(V(p)-V(l))^2}{\Delta V^2}\right) {\rm d}l, \qquad (3)$$

where $X_{\rm M}$ – methanol abundance relative to H_2, it was constant and equal to 10^{-6}; $L(p)$ – extension of the disc region with potential for maser formation along the line of sight at the given impact parameter p; f – a factor that accounts for decrease of the optical depth τ due to the turbulent motions in the disc (see below); ΔV – maser linewidth was equal to commonly observed value of 0.5 km s^{-1}; $n_{\rm H}(l)$ – hydrogen number density at a given distance l along the line of sight; ϵ^{-1} – beaming factor that is the ratio of the radial to tangential optical depths, it was constant and equal to 5; $V(p)$ and $V(l)$ – gas velocities at the given impact parameter and distance l along the line of sight, respectively. We assumed that the turbulent motions in the disc are of quasi-Kolmogorov type similar to those considered in Sobolev, Wallin & Watson (1998) and Wallin, Watson & Wyld (1998). For our calculation we adopted the value of $f = 0.69$ which corresponds to the maximum value obtained by Sobolev et al. (1998). Gas velocities were obtained assuming Keplerian motion for the accretion disc around the binary. We considered only impact parameters exceeding 10 au.

The pumping radiation at considered impact parameters was computed with CLOUDY.

Optical depths computed for $\alpha = 0.00008$ and 0.05 are presented in Figs 8 and 9, respectively. In order to characterize the excitation of the maser transitions we present in these figures an excitation factors (originally 'correction factors for stimulated emission') C computed according to Goldberg (1966):

$$C = 1 - \exp\left(-\frac{h\nu}{k_{\rm B} T_{\rm ex}}\right), \qquad (4)$$

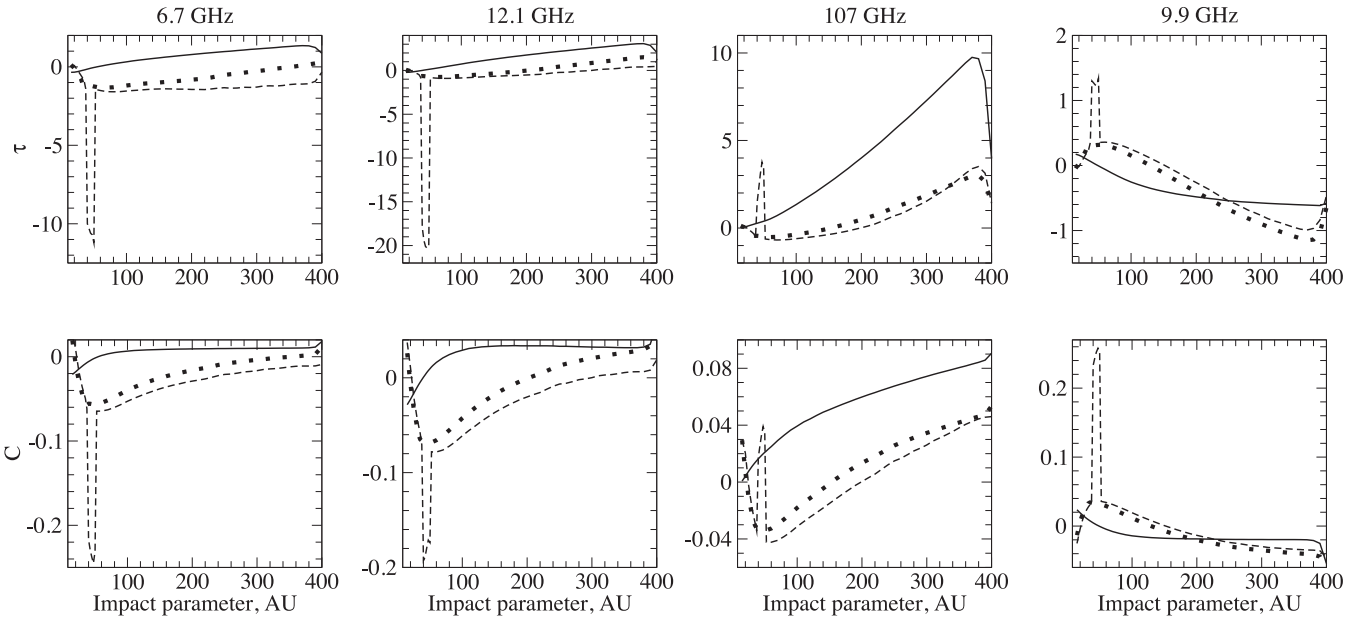

Figure 8. Maser optical depths τ and excitation factors C computed for disc models with $\alpha = 0.00008$. Solid line – under the MISO conditions; dotted line – shocked gas layer with $n_{\rm H} = 10^{13.32}$ cm^{-3} is located in the disc centre; dashed line – shocked gas layer with $n_{\rm H} = 10^{13.62}$ cm^{-3} is located in the disc centre. The negative optical depth means that there is a maser amplification in a given transition, while the positive value means that there is an absorption in maser transition.

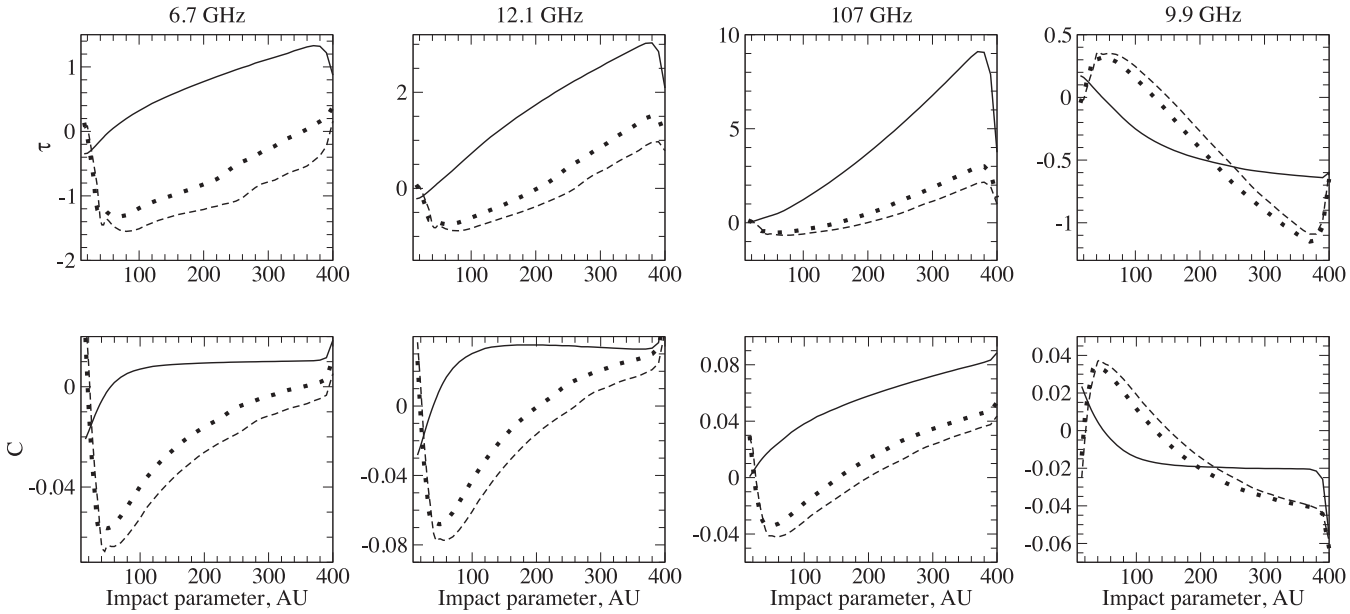

Figure 9. Same as Fig. 8 but for disc models computed with $\alpha = 0.05$.

where h – Planck constant; ν – frequency of the maser transition; $T_{\rm ex}$ – excitation temperature. We use the C factor because it has not singularities. Negative values of the optical depth and excitation factor mean that there is a maser amplification in a given transition, while the positive values mean that there is an absorption in this transition. The decrease of the optical depth from -1 to -10 corresponds to maser brightness increase by about four orders of magnitude. From Figs 8 and 9 it could be seen that three disc regions could be distinguished depending on the maser brightness behaviour under the MISO and MMISS conditions.

The first region of the disc is located in the range of impact parameters from 12 to 50 au. The behaviour of the maser brightness in this range of impact parameters considerably depends on the viscosity of the disc material. In this disc area under the MISO conditions the optical depth and C for masers at 6.7 and 12.1 GHz are negative, while τ and C for 9.9 GHz transition are positive. In the MMISS τ and C values for 6.7 and 12.1 GHz masers decrease, while at 9.9 GHz τ and C values increase. This effect greatly depends on the viscosity in the disc. When the viscosity is low the increase of τ and C values for 6.7 and 12.1 GHz transitions under the MMISS conditions is much more pronounced in comparison with the case when the viscosity is high. The brightness of 6.7 and 12.1 GHz masers could increase during the MMISS event by about 4 and 8 orders of magnitude, respectively, if $\alpha = 0.00008$, and only by about 1 order of magnitude if $\alpha = 0.05$.

Within the first region of the disc τ and C values for 107 GHz transition under the MISO conditions are mostly positive, i.e. the transition is quasi-thermally excited. At $p < 30$ au the 107 GHz transition is considerably overheated: C decreases and approaches 0, excitation temperature exceeds 1000 K and is considerably higher than the gas kinetic temperature which ranges in this region from 200 to 400 K. If the viscosity in the disc is low the brightness of 107 GHz maser is sensitive to the density of the shocked gas layer. The brightness of 107 GHz maser can experience decrease under the MMISS conditions if the shocked gas density is high.

The second region of the disc corresponds to impact parameters of 50–200 au. In this disc region τ and C values for 6.7, 12.1 and 107 GHz transitions are positive under the MISO conditions and become negative in the MMISS. Values of τ and C under the MISO conditions are positive for 9.9 GHz transition. In the MMISS τ and C values for 9.9 GHz transition remain negative and decrease their absolute values at $150 < p < 200$ au. This means that under the MMISS conditions in the range of impact parameters $150 < p < 200$ au the 9.9 GHz transition remains maser which decreases its brightness. In the outer parts of this disc region the decrease of the brightness of 9.9 GHz maser becomes pronounced only when the increase of the column density $N_{\rm gas}$ is close to its maximum value. According to Sytov et al. (2009) this maximum value is about 100 and for our considered model parameters this value corresponds to the shocked gas density of $n_{\rm H} = 10^{13.62}$ cm^{-3}. In the range of impact parameters from 50 to 150 au τ and C values for 9.9 GHz transition under the MMISS conditions become positive.

The third region of the disc corresponds to impact parameters of 200–400 au and differs from two inner regions by behaviour of the maser brightness of 9.9 GHz transition. In contrast to behaviour of the 9.9 GHz maser formed in the second region, τ and C values for 9.9 GHz maser transition remain negative and increase their absolute values under the MMISS conditions. In our model the brightness of 9.9 GHz maser in this disc region increased by about two times in the MMISS.

We also made calculations for other values of the beaming factor in the range from 1 to 25. The behaviour of τ and C values remained the same.

4 CONCLUSIONS

Using simple model we have shown that in the circumbinary accretion disc with the structure similar to the one presented by Sytov et al. (2011) the illumination of the disc by the bow shock hot material led to the variation of the dust temperature in the disc and considerably increased probability of the maser flare in the disc. The influence of the disc illumination by bow shock material on the maser brightness in the disc depends on the density of the shocked

material. In this study we considered the illumination by the material in the bow shock base originating close to the massive component surface. The appearance of the bow shock base in the line between considered position and the disc centre corresponds to the maximum rise of column density $N_{\rm gas}$ (given in Section 2.1) and leads to considerable increase of the radiation luminosity in the considered part of the disc. This radiation luminosity decreases while the spiral shock rotates and $N_{\rm gas}$ decreases. According to Sytov et al. (2009) $N_{\rm gas}$ rapidly increases and then slowly decays while the spiral shock rotates. We speculate that the maser brightness traces the $N_{\rm gas}$ change with the orbital phase reproducing characteristic features of the maser flare pattern in G9.62+0.20 and G351.42+0.64, and some other sources: rapid rise and relatively slow decay (Goedhart, Gaylard & van der Walt 2003, 2004; van der Walt, Goedhart & Gaylard 2009). In the paper of Sytov et al. (2009) it is shown that the pattern of $N_{\rm gas}$ variation depends on inclination angle of the binary, and the maser flare pattern can change accordingly.

In our model the probability of the maser flare in the disc area close to its centre depends on viscosity in the disc which is described by parameter α. When the viscosity is relatively low ($\alpha = 0.00008$) in the narrow disc area (15–50 au from the disc centre) the MMISS event can create a difference between the gas and dust temperatures up to $\sim$100 K. As a result, under the MMISS conditions the 6.7 and 12.1 GHz maser brightness in this disc area is much higher when the viscosity is low compared to the case when the viscosity is relatively high ($\alpha = 0.05$) and the great temperature difference does not occur.

When the disc viscosity is low the brightness of 107 GHz maser formed at impact parameters 12–50 au under the MMISS conditions strongly depends on the shocked gas density. When shocked density is maximum among the considered in this study, the brightness of 107 GHz maser is lower compared to the case when the shocked gas density is lower. Thus, while the spiral shock rotates and the column density increases there could be dips of the 107 GHz maser brightness under the MMISS conditions.

The 9.9 GHz maser in our model attains its maximum brightness at greater distances from the disc centre than other masers considered in this study. This means that the maser at 9.9 GHz can be observed at positions and velocities different from those of the 6.7, 12.1 and 107 GHz masers formed in the same object. Brightness of the 9.9 GHz maser formed at impact parameters 50–200 au decreases under the MMISS conditions. The effect strongly depends on the shocked gas density and becomes less pronounced with the distance from the centre, disappearing at 200 au.

The period of maser flares in our model is equal to the binary orbital period. If the binary consists of two massive stars then one can expect that the period of maser flares will be a half of the orbital period. The amplitude of the periodic flares is sensitive to variations in the shocked gas density and local parameters in the disc region where the masers are formed. The 6.7 and 12.1 GHz transitions show almost the same dependence of the maser brightness on the illumination (MMISS or MISO) conditions. The 107 and 9.9 GHz transitions can display flares or dips with the same period depending on the disc properties.

In this paper we considered stable axisymmetric disc model with monotonous dependence of parameters on the distance from the centre. Real discs are inhomogeneous. Parameters of the discs around binary systems as well as those of the binary systems are subject to time variations. This can result in the changes of variability patterns of different transitions with time.

Episodic increases of accretion rate represent another cause of the increase of stellar luminosity and gas density in the spiral shock. This can produce an effect similar to the MMISS event. According to our calculations the variation of the luminosity by about one and a quarter order of magnitude causes considerable changes of the brightness of masers formed in the accretion disc. We did not consider changes of the accretion rate but one has to expect that similar variation of the luminosity due to episodic changes of accretion rate can lead to episodic flares/dips of masers.

ACKNOWLEDGEMENTS

We are grateful to D. V. Bisikalo and M. A. Voronkov for useful comments.

REFERENCES

Araya E. D., Hofner P., Goss W. M., Kurtz S., Richards A. M. S., Linz H., Olmi L., Sewiło M., 2010, ApJ, 717, L133
Artymowicz P., Lubow S. H., 1994, ApJ, 421, 651
Baldwin J. A., Ferland G. J., Martin P. G., Corbin M. R., Cota S. A., Peterson B. M., Slettebak A., 1991, ApJ, 374, 580
Castelli F., Kurucz R. L., 2004, preprint (astro-ph/0405087)
Caswell J. L., 2013, in Wong T., Ott J., eds, Proc. IAU Symp. 292, Molecular Gas, Dust, and Star Formation in Galaxies. Cambridge Univ. Press, Cambridge, p. 79
Cragg D. M., Sobolev A. M., Godfrey P. D., 2005, MNRAS, 360, 533
De Buizer J. M., Redman R. O., Longmore S. N., Caswell J., Feldman P. A., 2009, A&A, 493, 127
Edris J. M., Fuller G. A., Cohen R. J., Etoka S., 2005, A&A, 434, 213
Ferland G. J. et al., 2013, Rev. Mex. Astron. Astrofis., 49, 137
Goedhart S., Gaylard M. J., van der Walt D. J., 2003, MNRAS, 339, L33
Goedhart S., Gaylard M. J., van der Walt D. J., 2004, MNRAS, 355, 553
Goedhart S., Gaylard M. J., van der Walt D. J., 2005a, Ap&SS, 295, 197
Goedhart S., Minier V., Gaylard M. J., van der Walt D. J., 2005b, MNRAS, 356, 839
Goedhart S., Maswanganye J. P., Gaylard M. J., van der Walt D. J., 2014, MNRAS, 437, 1808
Goldberg L., 1966, ApJ, 144, 1225
de Castro Gómez A. I., López-Santiago J., Talavera A., Sytov A. Yu., Bisikalo D. V., 2013, ApJ, 766, 62
Green S. D., Bolina A. S., Chen R., Collings M. P., Brown W. A., McCoustra M. R. S., 2009, MNRAS, 398, 357
Grevesse N., Sauval A. J., 1998, Space Sci. Rev., 85, 161
Hollenbach D., Johnstone D., Lizano S., Shu F., 1994, ApJ, 428, 654
Ilee J. D. et al., 2013, MNRAS, 429, 2960
Inayoshi K., Sugiyama K., Hosokawa T., Motogi K., Tanaka K. E. I., 2013, ApJ, 769, L20
Krumholz M. R., Klein R. I., McKee C. F., Offner S. S. R., Cunningham A. J., 2009, Science, 323, 754
Lang K. R., 1980, Astrophysical Formulae. A Compendium for the Physicist and Astrophysicist. Springer-Verlag, Berlin
Lanz T., Hubeny I., 2003, ApJS, 146, 417
McClure M. K. et al., 2013, ApJ, 775, 114
Menten K. M., Reid M. J., Pratap P., Moran J. M., Wilson T. L., 1992, ApJ, 401, L39
Minier V., Booth R. S., Conway J. E., 2000, A&A, 362, 1093
Moscadelli L., Goddi C., 2014, A&A, 566, 30
Nakagawa N., 1980, in Andrew B. H., ed., Proc. IAU Symp. 87, Interstellar Molecules. Reidel, Dordrecht, p. 365
Norris R. P. et al., 1998, ApJ, 508, 275
Ochi Y., Sugimoto K., Hanawa T., 2005, ApJ, 623, 922
Osterbrock D. E., Tran H. D., Veilleux S., 1992, ApJ, 389, 305
Ostrovskii A. B., Sobolev A. M., 2002, in Migenes V., Reid M. J., eds, Proc. IAU Symp. 206, Cosmic Masers: From Protostars to Black Holes. Astron. Soc. Pac., San Francisco, p. 183
Preibisch T., Ratzka T., Gehring T., Ohlendorf H., Zinnecker H., King R. R., McCaughrean M. J., Lewis J. R., 2011, A&A, 530, A40

Rubin R. H., Simpson J. P., Haas M. R., Erickson E. F., 1991, ApJ, 374, 564
Rubin R. H., Dufour R. J., Walter D. K., 1993, ApJ, 413, 242
Shakura N. I., Sunyaev R. A., 1973, A&A, 24, 337
Slysh V. I., Kalenskiĭ S. V., Val'tts I. E., 2002, Astron. Rep., 46, 49
Sobolev A. M., Deguchi S., 1994, A&A, 291, 569
Sobolev A. M., Cragg D. M., Godfrey P. D., 1997, MNRAS, 228, L39
Sobolev A. M., Wallin B. K., Watson W. D., 1998, ApJ, 498, 763
Sobolev A. M. et al., 2007, in Chapman J. M., Baan W. A. eds, Proc. IAU Symp. 242, Astrophysical Masers and Their Environments. Cambridge Univ. Press, Cambridge, p. 81
Sugiyama K. et al., 2014, A&A, 562, A82
Sytov A. Yu., Bisikalo D. V., Kaigorodov P. V., Boyarchuk A. A., 2009, Astron. Rep., 53, 428
Sytov A. Yu., Kaigorodov P. V., Fateeva A. M., Bisikalo D. V., 2011, Astron. Rep., 55, 793
Szymczak M., Wolak P., Bartkiewicz A., 2014, MNRAS, 439, 407
Torstensson K. J. E., van Langevelde H. J., Vlemmings W. H. T., Bourke S., 2011, A&A, 526, 9
van der Walt D. J., 2011, AJ, 141, 152
van der Walt D. J., Sobolev A. M., Butner H., 2007, A&A, 464, 1015
van der Walt D. J., Goedhart S., Gaylard M. J., 2009, MNRAS, 398, 961
van Hoof P. A. M., Weingartner J. C., Martin P. G., Volk K., Ferland G. J., 2004, MNRAS, 350, 1330
Voronkov M., Sobolev A. M., Ellingsen S., Ostrovskii A., Alakoz A., 2005, Ap&SS, 295, 217
Wallin B. K., Watson W. D., Wyld H. W., 1998, ApJ, 495, 774
Walsh A. J., Burton M. G., Hyland A. R., Robinson G., 1998, MNRAS, 301, 640
Wilson T. L., Walmsley C. M., Jewell P. R., Snyder L. E., 1984, A&A, 134, L7

APPENDIX A

We have changed the standard behaviour of two CLOUDY commands. The first command is 'Hextra SS' and it is used to include heating due to viscous dissipation. We made so that the heating rate introduced by this command is varied not only due to gas pressure variation but also with the radius from the disc centre. So, the third argument of this command became unimportant.

The second command is 'save transmitted continuum'. This command allows to save the sum of stellar radiation diffused through the surrounding gas and the radiation of the surrounding gas. We made so that before the summation of these two types of radiation the diffused stellar radiation is multiplied by the covering factor.

We also have added the new command 'trace OCCNUM' that allowed to save photon occupation numbers at given distances from the disc centre. Parameters of this command are the number of points in the disc for which occupation numbers should be saved and following list of distances from the disc centre in au.

To compute physical conditions in the disc in the MISO and with $\alpha = 0.00008$ the CLOUDY input was the following:

```
table star Tlusty OSTAR 3-dim temp=29000
log(g)=4.2 logZ=0.0
luminosity 4.155171131720616 solar
table star atlas odfnew 3-dim temp=20000
log(g)=4.2 logZ=0.0
luminosity 3.240853810488137 solar
cosmic rays background
abundances H  II region no grains
grains Orion function
cylinder log semi height=12.75471480186691
radius 13.45368480620293 16.1749254129166
covering factor 0.09805806756909208
hden 9.8, power =-1.0
iterate 10
stop temperature 3 K linear
set nend 3000
set nchrg 5
age 50 days
set didz -3
set trimming -10 upper
set trimming -14 lower
Hextra SS 0.00008 20 2.78e13
trace OCCNUM 55 10. 15. 20. 25. 30. 32.5 35. 37.5
40. 42.5 45. 47.5 50. 52.5 55. 60. 70. 80. 90.
100. 110. 120. 130. 140. 150. 160. 170. 180. 190.
200. 210. 220. 230. 240. 250. 260. 270. 280. 290.
300. 310. 320. 330. 340. 350. 360. 370. 380. 390.
400. 420. 440. 460. 480. 500.
save physical conditions last ''PhysCond.dat''
save grain temperature last ''GrainTemp.dat''
save grain abundance last ''GrainAbund.dat''
save grain heating last ''GrainHeat.dat''
save element last hydr ''Hion.dat''
save continuum last ''Cont.dat''
save H2 temperatures last ''H2Temp.dat''
save molecules last ''Mole.dat''
```

To compute the radiation from the shocked gas layer with $n_{\rm H} = 10^{13.62}$ cm^{-3} the CLOUDY input was the following:

```
table star Tlusty OSTAR 3-dim temp=29000
log(g)=4.2 logZ=0.0
luminosity 4.155171131720616 solar
cosmic rays background
abundances H  II region no grains
cylinder log semi height=11.51848788013858
radius 11.51848788013858 12.47595540770966
covering factor 0.5
hden 13.621
constant temperature, t=30222K linear
iterate 20
stop temperature 3 K linear
age 50 days
print heating
print ages
save physical conditions last ''PhysCond.dat''
save element last hydr ''Hion.dat''
save continuum last ''Cont.dat''
save transmitted continuum last ''radiation.txt''
```

To compute physical conditions in the disc in the MMISS, with $\alpha = 0.00008$ and with shocked gas layer density of $10^{13.62}$ cm^{-3} the CLOUDY input was (comments begin with #) the following:

```
table read ''radiation.txt''
nuL(nu) = 38.71516846700204 at 0.996143 Ryd
# when the shocked gas density equals to
# 10^(13.32) cm^(-3)
# the latter command should be replaced by
# nuL(nu) = 38.54965303728508 at 0.996143 Ryd
cosmic rays background
abundances H  II region no grains
grains Orion function
cylinder log semi height=12.75471480186691
radius 13.45368480620293 16.1749254129166
covering factor.2181456377060064
hden 9.8, power =-1.0
iterate 10
stop temperature 3 K linear
```

```
set nend 3000
set nchrg 5
age 50 days
set didz -3
set trimming -10 upper
set trimming -14 lower
Hextra SS 0.00008 20 2.78e13
print heating
print ages
trace OCCNUM 55 10. 15. 20. 25. 30. 32.5 35. 37.5
40. 42.5 45. 47.5 50. 52.5 55. 60. 70. 80. 90.
100. 110. 120. 130. 140. 150. 160. 170. 180. 190.
200. 210. 220. 230. 240. 250. 260. 270. 280. 290.
300. 310. 320. 330. 340. 350. 360. 370. 380. 390.
400. 420. 440. 460. 480. 500.
save physical conditions last ''PhysCond.dat''
save grain temperature last ''GrainTemp.dat''
save grain abundance last ''GrainAbund.dat''
save grain heating last ''GrainHeat.dat''
save element last hydr ''Hion.dat''
save continuum last ''Cont.dat''
save H2 temperatures last ''H2Temp.dat''
save molecules last ''Mole.dat''
```

This paper has been typeset from a TEX/LATEX file prepared by the author.